Use of VAS Data to Diagnose the Mesoscale Environment of Convective Storms

RAYMOND M. ZEHR, JAMES F. W. PURDOM, JOHN F. WEAVER AND ROBERT N. GREEN

NOAA/NESDIS/Regional and Mesoscale Meteorology Branch, Cooperative Institute for Research in the Atmosphere (CIRA), Colorado State University, Fort Collins, Colorado

ABSTRACT

The utility of VISSR Atmospheric Sounder (VAS) retrieval datasets for mesoscale analysis is explored. A detailed mesoscale air mass analysis method is presented in which VAS soundings, satellite imagery, and conventional surface data are used to diagnose mesoscale differences in air mass character. Comparisons are made with radiosonde observations of the same air mass differences. A mesoscale air mass analysis is presented with a discussion of the role that the various air masses play in subsequent convective development.

In a second technique, several VAS-derived thermodynamic parameters, such as positive and negative buoyant energy, are shown to be well suited to operational forecasting of convective storm development and evolution. The derivation of these parameters and their applications in forecasting are illustrated.

1. Introduction

Convective storms play an important role across many spatial and temporal scales in meteorology. Locally, convective storms may initiate weather-related events that affect everyday life. While thunderstorms provide much needed water for agricultural purposes, they can also produce tornadoes, hail, flash floods, downbursts, and lightning, all of which pose serious threats to life and property. On this convective scale, improvements in short-range forecasting (often termed nowcasting) are much needed (Browning, 1982). However, before precise local forecasting becomes a reality, an improvement in the understanding of convective storm genesis and development is required.

Most of the available information on convective storm development and intensification is focused on either the large-scale conditions favorable for development (Miller, 1972) or on the individual convective storm (Byers and Braham, 1949; Brandes, 1978). More is known about synoptic-scale development and cloud microphysics than about the mesoscale, which remains both poorly measured and poorly understood (NCAR, 1984). This lack of mesoscale knowledge has been due mainly to a gap in meteorological observing capability in the era prior to the high resolution geostationary satellite. However, with the advent of the Geostationary Operational Environmental Satellites (GOES) this capability has become available, and many advances have been made in the area of mesoscale meteorology

through the interpretation of satellite cloud imagery (Purdom, 1982).

Additional mesoscale information became available in 1980 when the VISSR (Visible and Infrared Spin Scan Radiometer) Atmospheric Sounder (VAS) instrument was placed in geostationary orbit. VAS has the ability to provide frequent sounding data over mesoscale areas (Suomi et al., 1971). Sounders similar to VAS have been a part of NOAA's polar-orbiting satellite observing system since the early 1970s. Therefore, algorithms to compute vertical profiles of temperature and humidity from satellite-measured radiances had been developed many years earlier (Chahine, 1968; Smith, 1970). Profiles such as these, referred to as retrievals, are available from VAS. Satellite-measured radiances in combination with "first-guess" fields or statistical information from conventional data are used to compute the retrievals (satellite soundings).

Smith et al. (1982) have demonstrated the potential of using VAS-generated parameters to detect features important to severe thunderstorm development. More recently, VAS retrievals have been used to support severe thunderstorm forecasters at the National Severe Storms Forecast Center (NSSFC; Wade et al., 1985) and for tropical cyclone applications at the National Hurricane Center (Velden et al., 1984). Another application of VAS data has been the initialization of mesoscale numerical models (Kreitzberg, 1976; Mills and Hayden, 1983; Cram and Kaplan, 1985).

Although VAS retrieval data have been available to forecasters at the NSSFC for several years, their operational use has been somewhat limited, due to the usual problems associated with introducing new information to forecasters constrained by operational duties coupled with the inconsistent availability of VAS

Corresponding author address: Dr. Raymond M. Zehr, NOAA/NESDIS/RAMM, Dept. of Atmospheric Science, Colorado State University, CIRA Bldg., Foothill Campus, Fort Collins, CO 80523.

TABLE 1. VAS instrument characteristics.

Spectral channel	Central wavelength (μm)	Absorbing constituent	Weighting function		Surface or cloud emission effect
			Peak level (mb)	Representative thickness (mb)	
1	14.7	CO_2	70	150–10	usually none
2	14.5	CO_2	125	200–50	nothing below 500 mb
3	14.2	CO_2	200	500–50	nothing below 800 mb
4	14.0	CO_2	500	800–300	weak
5	13.3	CO_2	920	SFC–500	moderate
6	4.5	CO_2	850	SFC–500	moderate
7	12.7	H_2O	surface	SFC–700	strong
8	11.2	window	surface	—	strong
9	7.2	H_2O	600	800–400	weak at surface
10	6.7	H_2O	400	700–250	nothing at surface
11	4.4	CO_2	300	800–100	weak
12	3.9	window	surface	—	strong

data. The inconsistent availability of VAS data has mainly been due to the unfortunate reality of having only one fully operational GOES satellite during the period August 1985 to March 1987 and the inability of the current generation GOES satellites to do both sounding and imaging simultaneously.

Mostek et al. (1986) concluded that VAS data, when appropriately combined with conventional surface and radiosonde data, can help resolve some of the processes which lead to the development and maintenance of convective storm systems. Their paper presents a quantitative assessment of temperature and moisture structures previously described with VAS imagery by Chesters et al. (1983) and Petersen et al. (1984). In this study, VAS data are used to diagnose the differences among air masses which influence convective storm development. The emphasis is on assessing the potential of mesoscale air masses to support deep convective clouds, severe thunderstorms, and mesoscale convective systems (MCS).

2. VAS data

a. The VAS instrument

The sounder portion of the VAS instrument measures outgoing radiation from the earth–atmosphere system in 12 different spectral bands (channels). Characteristics of individual channels are given in Table 1, and their weighting functions for the U.S. Standard Atmosphere are shown in Fig. 1. These weighting functions illustrate the sensitivity of each channel to atmospheric height (pressure) and thus the vertical resolution of VAS data. In terms of horizontal resolution, all twelve channels can resolve 13.8 km while 6.9 km "fields of view" are available from six of the channels. The VAS instrument characteristics, calibration, and performance details are given in Menzel et al. (1981).

The VAS instrument can be operated in one of three modes: 1) a normal VISSR mode for routine visible and infrared imaging, 2) a dwell sounding mode which uses all or most of the sounder channels to collect data for retrievals, and 3) a multispectral imaging (MSI) mode in which VISSR data plus two additional VAS channels are sampled. The MSI mode allows frequent-interval water vapor imagery. The three modes of operation are not independent; when the satellite is operated in one mode, data from the other modes are not available. When VAS is operated in the dwell sounding
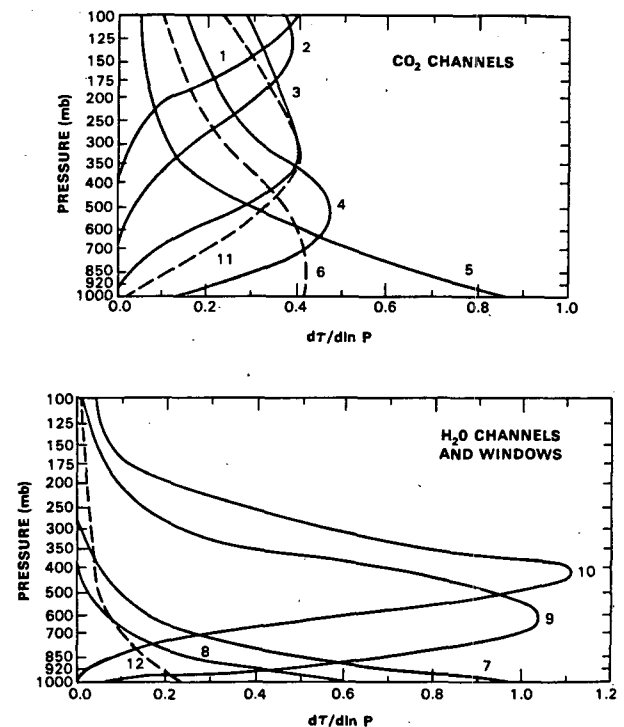

FIG. 1. Radiance weighting functions of the VAS channels for the U.S. Standard Atmosphere. Dashed lines indicate the shorter wavelengths, which may be influenced by reflected sunlight.

mode, data from the various channels may be viewed individually or processed to produce mesoscale soundings.

b. Retrieval algorithms

Radiance measurements from the various VAS channels are used to compute (retrieve) vertical profiles of temperature and humidity. Two types of retrieval algorithms have been employed to derive VAS soundings. A physical method based on an iterative solution of the radiative transfer equation is outlined by Smith (1983), and an empirical method based on statistical regression techniques is described by Smith et al. (1970) and Lee et al. (1983). The VAS retrievals shown in this paper were obtained in near real time from the Cooperative Institute for Meteorological Satellite Studies (CIMSS) at the University of Wisconsin. These datasets were produced routinely in support of both National Weather Service operations and research field programs. VAS soundings were computed at approximately 80-km resolution by eliminating cloud contaminated fields of view and averaging pixels to increase the signal-to-noise ratio. Each VAS retrieval consists of geopotential height, temperature, and dewpoint at constant pressure levels.

The VAS soundings for this case study were computed with the physical retrieval algorithm described by Hayden and Menzel (1986) and Smith and Woolf (1984). This new method calculates temperature and moisture profiles simultaneously. It was designed to correct some of the problems of the original physical formulation (Smith, 1983), particularly the large errors in moisture content. The first-guess fields used in the computations were the LFM (Limited-area Fine Mesh) model forecasts.

This paper does not deal with evaluation of retrieval algorithms or data resolution, but rather with the application of VAS data to meteorological problems. However, the validity of VAS soundings and retrieval methods is an important topic on which additional research is needed. A few comments and findings pertinent to retrieval algorithm evaluation and VAS–radiosonde sounding comparisons are included in section 4.

c. Microcomputer workstation

One of the ongoing research goals of the authors during the past several years has been the development of a microcomputer-based meteorological workstation suitable for research and operations. This system has been used for real-time support of the Oklahoma–Kansas PRE-STORM (Preliminary Regional Experiment for Stormscale Operational and Research Meteorology) operations (Purdom et al., 1985; Green and Weaver, 1985) and was utilized for much of the research work described in this paper.

The hardware components are based on the IBM series of personal computers with peripherals from various manufacturers. The base processor is an IBM PC/XT with a 10 megabyte hard disk, 640K bytes of memory and a numeric processor to increase floating-point calculations speed. Two video monitor displays are used: 1) a monochrome screen which provides the text display for menus and alpha-numeric data, and 2) a color screen for graphical displays and imagery presentations. A dot matrix printer provides the capability of hardcopy of products displayed on either screen. Data transfer from the mainframe computer utilizes a 1200 baud automatic-dial modem connected to a standard telephone line. The workstation can be used for satellite image display and analysis of VAS retrievals. Various color enhancement, animation, and histogramming routines are also available. Additional details are given by Green et al. (1986).

d. VAS-derived products

The VAS retrieval datasets provide input to the workstation from which numerous constant level fields and derived quantities are generated and analyzed. A modified sounding analysis routine, originally designed for analysis of radiosonde observations, computes various parameters applicable to thunderstorm forecasting (Table 2 and Fig. 2). This routine requires 3–4 seconds per sounding to run on the IBM PC/XT. Although all variables in Table 2 have been analyzed and evaluated, the bulk thermodynamic parameters are the primary quantities of interest for this study. These parameters are computed from layer averages and thermodynamic diagram area (energy) averages, and therefore minimize a weakness of VAS retrievals—poor vertical resolution.

Convective storms derive most of their energy from the convective available potential energy (CAPE) of the prestorm environment (Normand, 1938; Haltiner and Martin, 1957; Moncrieff and Green, 1972). The CAPE is measured by integrating the positive temperature difference between a near surface-layer parcel displaced upward adiabatically without entrainment and the environmental temperature. This energy source, often referred to as buoyant energy (B) or "positive area," is easily computed from sounding data. Additionally, "negative areas" which must be overcome, either by lifting or by heating in order to realize the potential positive buoyant energy, can also be computed. For this paper, the lifted negative area (N) is defined as the negative buoyant energy that must be overcome for a parcel to ascend adiabatically to its level of free convection (LFC). The energy required to attain convective temperature defines the area to be overcome by heating (H), and is represented by the area between the environmental temperature and the dry adiabat of the convective temperature (Fig. 2).

The layer from the surface to a height of 1 km is used to represent the subcloud layer parcel. Therefore,

TABLE 2. Parameters derived from each VAS retrieval.

Type and name	Notation	Units	PC number and abbreviation		Comments
			Parcel definition		
1. Lowest kilometer dewpoint	$\overline{DP}_{0-1\ km}$	°C	77	0–1 km DEW PT	A mass weighted average computed from all interpolated levels with heights less than 1000 m above the surface is used to define a parcel.
2. Lowest kilometer temperature	$\bar{T}_{0-1\ km}$	°C			
3. Lowest kilometer mixing ratio	$\bar{r}_{0-1\ km}$	g kg^{-1}	78	0–1 km MIX RATIO	
			Parcel levels		
4. Height of lifting condensation level (LCL)	Z_{LCL}	m	79	LCL HT	The LCL height, pressure, temperature, and mixing ratio are computed exactly based on parcel definition.
5. Pressure of LCL	P_{LCL}	mb	80	LCL P	
6. Temperature of LCL	T_{LCL}	°C	81	LCL TEMP	
7. Mixing ratio of LCL	r_{LCL}	g kg^{-1}	82	LCL MIX	
8. LFC (level of free convection) pressure	P_{LFC}	mb	83	LFC P	The pressure level of the LFC, EL, and CCL are computed as the first interpolated level above their actual level. Therefore, there is an error of $\pm \Delta Z$, where ΔZ = interpolation increment.
9. EL (equilibrium level) pressure	P_{EL}	mb	84	EL P	
10. CCL (convective condensation level) pressure	P_{CCL}	mb	85	CCL P	The CCL is defined by the intersection of the lowest kilometer mixing ratio line and the temperature sounding line.
			Stability indices		
11. Lifted index	LI	°C	86	LIFTED INDEX	LI = $T_{500\ mb}$ − Parcel $T_{500\ mb}$
12. K index	K	°C	87	K INDEX	K = $(T_{850} - T_{500}) + DP_{850} + (700\ mb\ DP$ depression$)$
13. Totals − Totals		°C	88	TOT − TOT INDEX	Totals − Totals = $[(T_{850} - T_{500}) \times 2]$ − $(850\ mb\ DP$ depression$)$
			Thermodynamic energy parameters		
14. Positive buoyant energy	B	J kg^{-1}	89	POS BUOY	Thermodynamic energy parameters are computed as mass averages of appropriate temperature differences using all pertinent interpolated levels. Parameters 14, 15, 16 and 17 are determined by the parcel (parameters 1–3) and by the temperature sounding. Parameters 18 and 19 are determined by a parcel defined by parameters 3 and 20.
15. Negative buoyant energy (LCL to LFC)	$N_{LCL-LFC}$	J kg^{-1}	90	NEG E(LCL–LFC)	
16. Negative buoyant energy (surface to LCL)	$N_{SFC-LCL}$	J kg^{-1}	91	NEG E(SFC–LCL)	
17. Negative buoyant energy (total below LFC)	N	J kg^{-1}	92	TOT NEG E	
18. Additional heat energy required to reach convective temperature	H	J kg^{-1}	94	E TO CNVCT TEMP	
19. Positive buoyant energy from parcel at the CCL	B_{CCL}	J kg^{-1}	95	POS BUOY CCL	
			Additional thermodynamic parameters		
20. Convective temperature	T_c	°C	93	CONVECT TEMP	Convective temperature is defined as a surface temperature with the same potential temperature as the CCL.
21. Maximum possible updraft velocity	w_{max}	m s^{-1}	96	MAX V V	
22. Minimum wet-bulb potential temperature (θ_w)	$\theta_{w_{min}}$	°C	97	MIN THETA W	The maximum possible updraft velocity is based on the positive buoyant energy, B.

TABLE 2. (*Continued*)

Type and name	Notation	Units	PC number and abbreviation		Comments
23. Height of minimum θ_w	$HT_{\theta_{w_{min}}}$	m	98	HT MIN THETA W	
24. Wind directions at height of θ_w minimum	$bDIR_{\theta_{w_{min}}}$	deg	99	DIR MIN THETA W	
25. Wind speed at height of minimum θ_w	$SPD_{\theta_{w_{min}}}$	m s^{-1}	100	SPD MIN THETA W	
26. Height of 0°C wet-bulb temperature	$HT_{T_{w=0}}$	m	101	HT WB ZERO	
Wind parameters					
27. Mean wind direction in 3–10 km layer	$DIR_{3–10\ km}$	deg	102	MEAN DIR (3–10 km)	The mean wind is a mass weighted average. Heights refer to above the surface, not MSL.
28. Mean wind speed in 3–10 km layer	$SPD_{3–10\ km}$	m s^{-1}	103	MEAN SPD (3-10 km)	
Average magnitude of wind shear vector:					
29. 0–3 km layer		m s^{-1} km^{-1}	104	0–3 KM SHEAR	
30. 3–10 km layer		m s^{-1} km^{-1}	105	3–10 KM SHEAR	
Average turning of wind					
31. 0–3 km		deg km^{-1}	106	0–3 KM DIR TURN	
32. 3–10 km		deg km^{-1}	107	3–10 KM DIR TURN	
Combined parameter					
33. Mean Richardson number (Ri) from LCL to 10 km			108	RI	$Ri = \left(\dfrac{g}{\theta}\dfrac{\partial \theta}{\partial Z}\right)\Big/\left(\dfrac{\partial V}{\partial Z}\right)^2$

the average lowest kilometer temperature and mixing ratio define the adiabatic parcel ascent which, along with the environmental temperature profile, determines the bulk thermodynamic parameters: CAPE (*B*) and negative areas (*N* and *H*). As the lowest kilometer is heated, there is a resultant increase in CAPE. For some applications, it is advantageous to remove the diurnal heating and cooling effects on the positive area (e.g., the morning surface inversion). This can be done by introducing an additional CAPE parameter (B_{CCL}) defined by the lowest kilometer mixing ratio and the convective temperature (Fig. 2). This positive area represents parcel ascent from the convective condensation level (CCL). As the boundary layer is heated, *N* and *H* approach zero, and *B* approaches B_{CCL}. Therefore, B_{CCL} often allows an assessment of afternoon convective potential from morning soundings, while values of *B* may not.

The purpose of computing the thermodynamic parameters from VAS soundings is to aid the analysis of convective potential on mesoscale space and time scales. The CAPE parameters measure buoyant energy available to thunderstorm updrafts, while the negative area parameters measure the forcing required to initiate thunderstorms. Applications of the thermodynamic parameters are illustrated in section 3c.

3. The 21–22 June 1984 mesoscale convective system (MCS)—a case study

Several mesoscale convective systems developed in the Great Plains during the late afternoon and continued through the night of 21–22 June 1984. This case study will focus on one of those mesoscale convective systems which developed in Kansas. The primary goal of the case study is to illustrate the contribution of VAS soundings in assessing the mesoscale characteristics of the atmosphere over the central Great Plains.

a. Synoptic-scale setting

The 1200 UTC surface analysis, superimposed on the 1200 UTC infrared image in Fig. 3, depicted several features of interest. A cold front, which had pushed into the western Dakotas, trailed westward through central Wyoming, and a stationary front extended southeastward from central South Dakota to eastern Kansas. Showers and thundershowers were located along the front in both South Dakota and eastern Kansas. A lee trough extended from western South Dakota to a region of low pressure in southwest Kansas.

At upper levels over the central Great Plains, the flow pattern was generally weak (Fig. 4a). Winds at 500
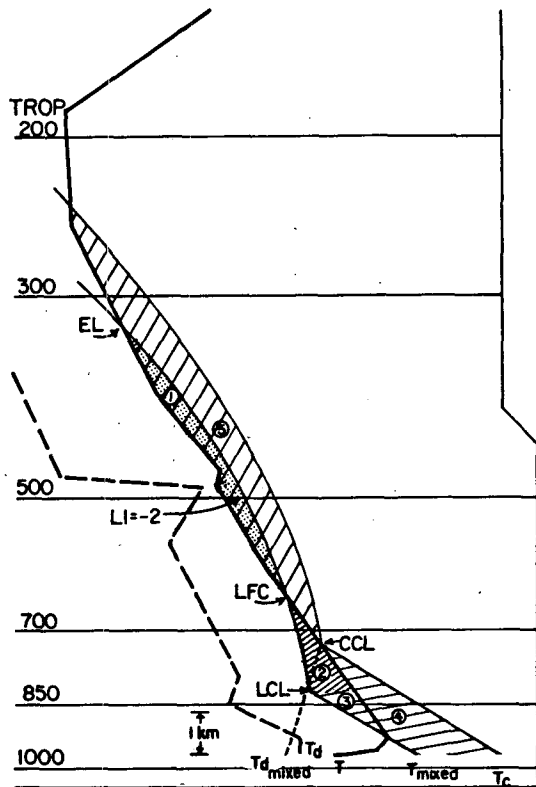
FIG. 2. Skew T–log$p$ diagram illustrating the bulk thermodynamic parameters computed from VAS retrievals. Circled numbers with shaded areas indicate: 1) positive buoyant energy, B (also referred to as CAPE, convective available potential energy); 2) negative buoyant energy, N, between LCL and LFC; 3) negative buoyant energy, N, between surface and LCL; 4) heating area, H, heat energy required to attain convective temperature (Tc); 5) positive area, B_{CCL}, positive buoyant energy with convective temperature.

mb were southwesterly at 10 m s^{-1} over Nebraska and Kansas, becoming light and variable further to the south. The 700- and 850-mb analyses showed anticyclonic flow over most of the south central plains. At 850 mb (Fig. 4b), a wind maximum (18 m s^{-1}) extended from southwest Texas to Kansas. Dewpoints at 850 mb in this flow ranged from 11° to 17°C. The morning MCS forecast by research forecasters suggested that storms in eastern Kansas would develop into a large MCS later in the day in response to the low-level jet in that area (Weather Research Program, 1984).

By early afternoon, satellite imagery revealed heavy cumulus cloud streets had formed in the unstable air near the 850 mb moist axis in Texas and Oklahoma (Fig. 5). The front which had previously been stationary had moved slowly northeastward as a warm front. However, sequential satellite imagery showed that the previous thunderstorm activity had remained behind. As the storms dissipated, they left a clear, stable air mass which gradually encompassed most of the eastern portion of Kansas. Similar rain-cooled air masses were found in the eastern Dakotas, extreme northeast Ne-

braska, and a small region along the western section of the Kansas–Nebraska border. New thunderstorm activity was forming in northern Oklahoma where the low-level moist flow intersected the boundary left by the earlier thunderstorm activity in eastern Kansas and Oklahoma.

b. Mesoscale analysis using VAS retrievals

VAS retrievals at approximately 80 km resolution were available at one- to three-hour intervals during the period from 1100 UTC 21 June to 1400 UTC 22 June 1984. After inspecting numerous fields derived from VAS soundings, such as geopotential heights and thicknesses, the most effective method of identifying mesoscale air mass features was found to be comparisons of individual VAS vertical profiles of temperature and dewpoint. In the procedure that was developed, adjacent retrievals with very small differences in temperature and dewpoint through the entire depth of the troposphere were grouped together as a first step in the mesoscale analysis. The result of such a grouping for 2318 UTC 21 June is shown by the blocky, shaded regions in Fig. 6. The unshaded areas are where retrievals did not fit into any particular group or were unavailable due to extensive cloud cover. The next step in the analysis was to locate more precisely the boundaries separating the mesoscale air masses. Cloud features in satellite images along with conventional surface and upper air analyses were used for this step. The heavy lines in Fig. 6 show those additions.

Several changes in the surface features had occurred since the midday analysis (Fig. 5). A dryline had formed
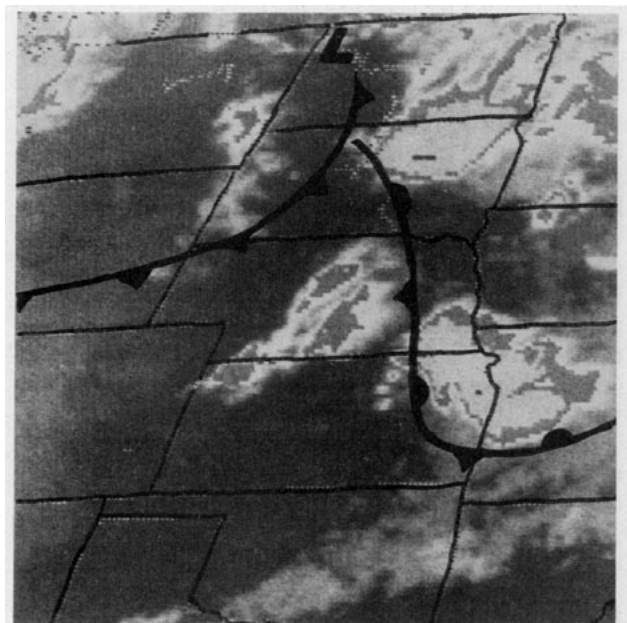

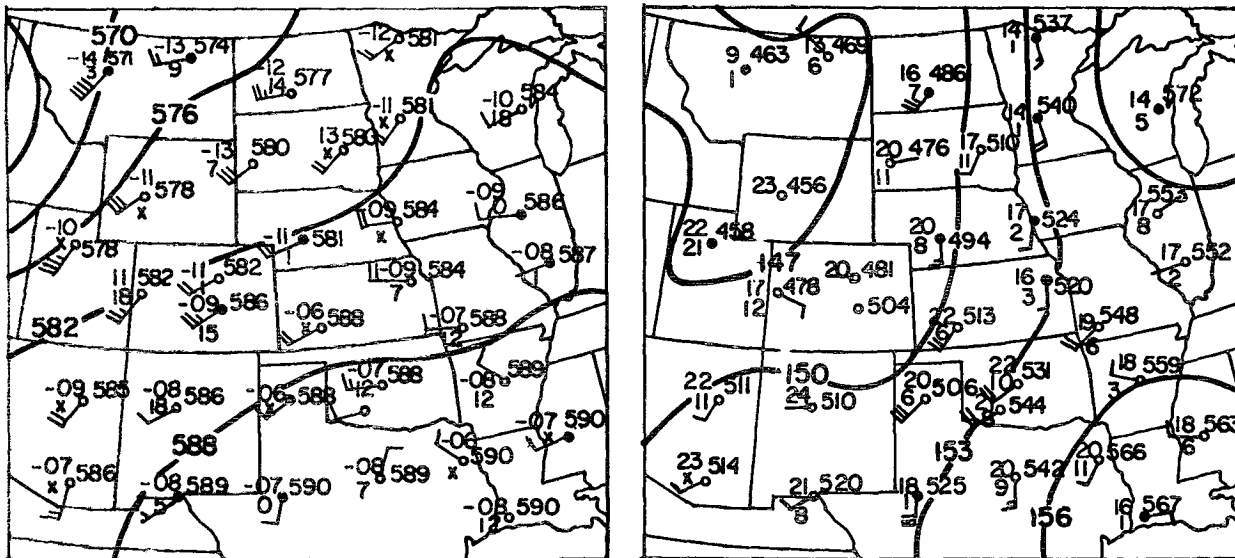FIG. 3. Enhanced infrared satellite image with surface analysis for 1200 UTC 21 June 1984.

FIG. 4. (a) 500-mb analysis and (b) 850-mb analysis for 1200 UTC 21 June 1984.

on the high plains due to diurnal heating and mixing, corresponding to the eastern edge of air mass 4 in Fig. 6. Meanwhile, the cold front in Wyoming and the Nebraska panhandle (Fig. 5) was very difficult to find at 2300 UTC, likely due to very strong surface heating. However, a frontal region in the middle and upper troposphere across southern Nebraska is shown by the dashed line in Fig. 6. This differentiates the boundary from the others (solid lines) which are lower tropospheric features. As will be noted later, boundaries between mesoscale air masses are often confined to a specific layer rather than through the entire depth of the troposphere.

Other boundaries are more readily seen on the satellite imagery. For example, the edge of cumuliform clouds aligned through central Kansas on the 2315 UTC satellite image in Fig. 7 marks the very distinct boundary between air masses 1 and 2 (Fig. 6). An arc cloud line (Purdom, 1973) can be seen in eastern Nebraska.

The additional mesoscale features revealed by the analysis method described above can be seen by comparing Fig. 6 with the conventional surface analysis in Fig. 8. The trough line corresponding to the boundary between air masses 1 and 2, and the warm front in Iowa and Missouri, are the only features in Fig. 8 that appear in the mesoscale air mass analysis (Fig. 6).

Further refinements could be made by devising techniques which incorporate any additional pertinent features identified when a radiosonde observation is available within a particular mesoscale air mass. For example, a shallow inversion layer might be identified as an additional air mass characteristic.

It is important to note that for the purposes of this paper, an air mass is defined as an area in which the atmosphere is uniform with regard to potential intensity of deep convective updrafts and the magnitude of forcing necessary to initiate convective clouds. This is more specific and concise than the conventional definition of an air mass described by a widespread body of air with approximately homogeneous temperature and moisture distribution in the horizontal. The newly defined air mass is more suited to analysis of mesoscale features and convective weather systems.

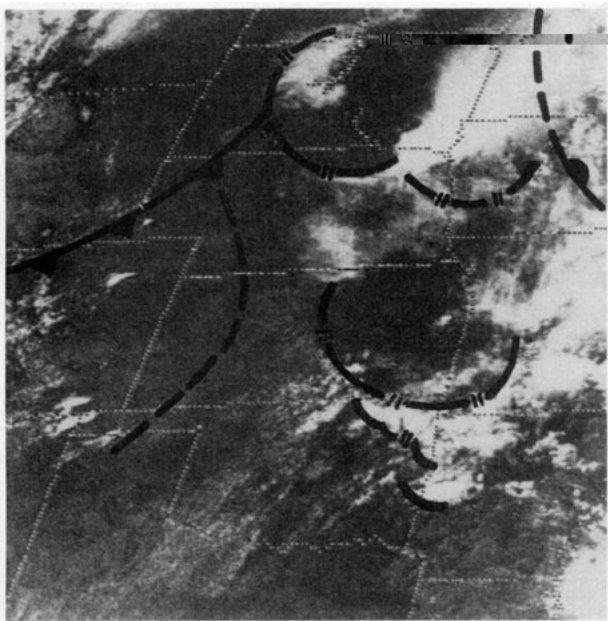Each of the seven air masses shown in Fig. 6 have

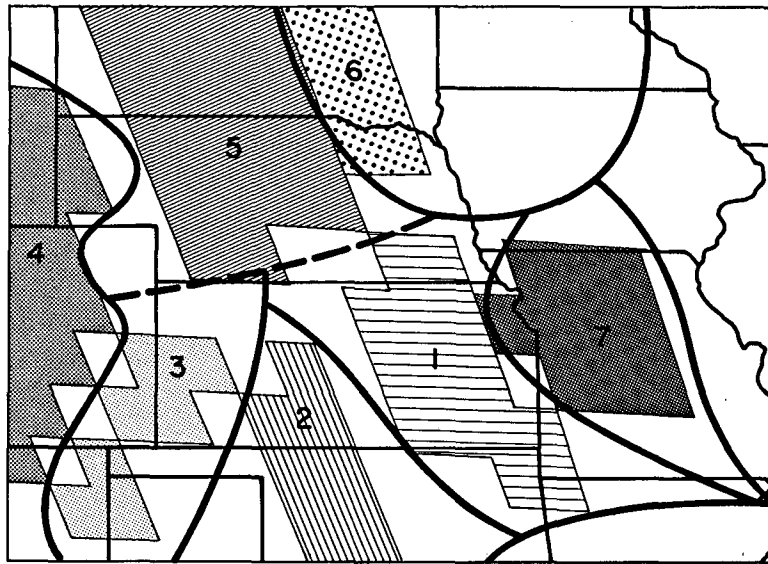FIG. 5. Visible satellite image from GOES-East for 1930 UTC 21 June 1984.

FIG. 6. Mesoscale air mass analysis at 2318 UTC 21 June 1984. The shaded regions depict the area covered by representative VAS retrievals within each air mass. Dashed lines indicate midtroposphere boundaries, and solid lines indicate lower troposphere boundaries.

specific differentiating characteristics with respect to their thermodynamic structure and convective potential. Information about the convective potential of each air mass is available from conventional surface and upper air observations and from satellite images. These characteristics are summarized in Table 3.

The VAS soundings provide additional information and reveal features unique to each air mass type which have important implications to the development and evolution of mesoscale convective systems. Figure 9 depicts air mass differences across several of the boundaries shown by representative VAS retrievals for different air mass pairs. Several radiosonde observations assigned to the air mass at their location are plotted as corresponding pairs in Fig. 10. The VAS-detected air mass differences in Fig. 9 are qualitatively similar
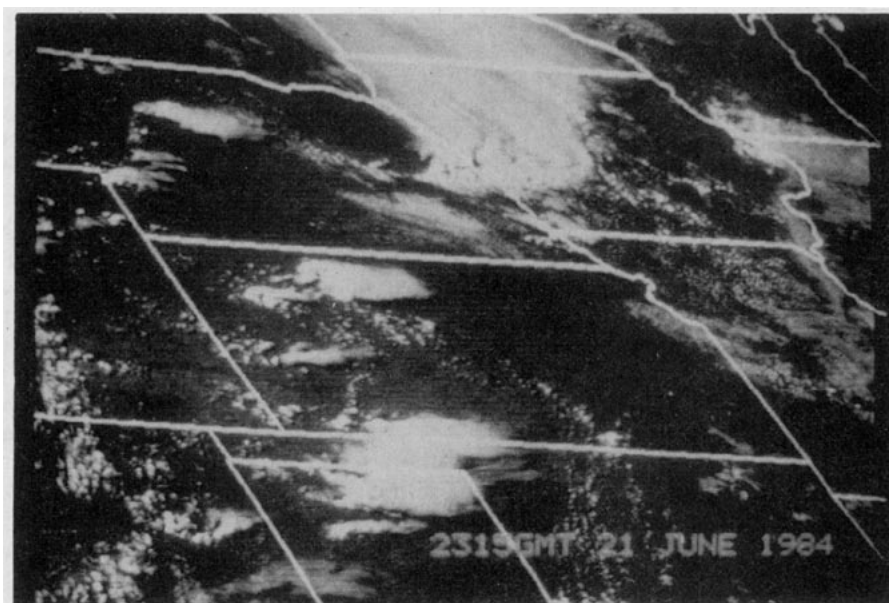

FIG. 7. Visible satellite image from GOES-West for 2315 UTC 21 June 1984.
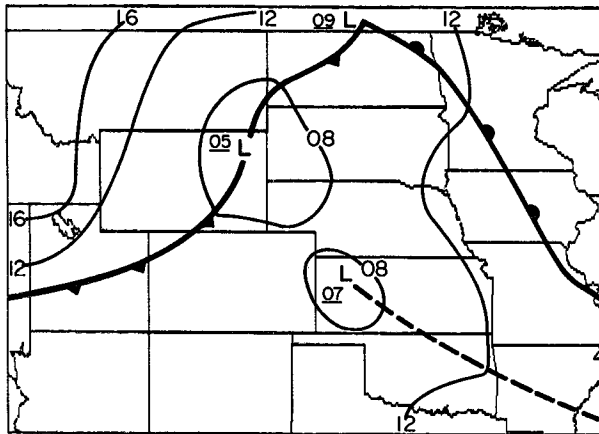
FIG. 8. Conventional surface analysis for 0000 UTC 22 June 1984.

to the differences measured by radiosondes in Fig. 10. Also, the specific characteristics of each air mass relevant to convective development are detected by both the radiosondes and VAS. The radiosondes add detail due to their better vertical resolution, while the VAS soundings reveal the horizontal extent of air masses.

Figures 9 and 10 illustrate important mesoscale characteristics of specific air masses. For example, air mass 1 has a significantly smaller lapse rate at the lower levels than air mass 2 (Figs. 9a and 10a). Air mass 1 in the satellite image (Fig. 7) is completely clear, in contrast to air mass 2 with numerous small cumulus and some cumulonimbus. This low-level lapse rate difference is seen between air masses 1 and 5 as well; however, there are also significant differences in the middle and upper troposphere temperature (Figs. 9b and 10b). The colder upper troposphere has important implications with regard to CAPE. Consider two subcloud layer parcels with identical temperature and mixing ratio (perhaps in air masses 2 and 5). The CAPE will be significantly larger in air mass 5 due to the colder temperature in the middle and upper troposphere (i.e., greater lapse rate).

A somewhat more complex situation is observed in the differences between air masses 5 and 6 (Figs. 9c and 10c). Air mass 6 has been modified by evaporative cooling and subsidence in response to a mesoscale convective system located in southern Iowa. The arc cloud line seen in the visible satellite image (Fig. 7) is aligned along a portion of the boundary between air masses 5 and 6. Figure 9c shows the VAS-detected differences between the two air masses, showing a cooler and drier air mass in the rain-cooled air. Figure 10c shows radiosonde observations at Omaha, Nebraska, before and after passage of the outflow boundary. The cool air is confined to a very shallow surface layer (600 m), and the air layer above it is warm and dry having undergone adiabatic descent (Fujita, 1963). Because of its poor vertical resolution, VAS is unable to detect the

thermodynamic characteristics of very shallow layers, such as the surface layer depicted in Fig. 10c.

To complete the analysis, brief descriptions of the vertical temperature and moisture profiles of air masses 3, 4 and 7 are required. These descriptions are based on surface observations and VAS soundings. Air mass 4 is very dry with insufficient moisture to support deep convective clouds. Air mass 3 is significantly drier in the subcloud layer than air mass 2, but enough moisture is present to support cumulonimbus cloud development (Fig. 7). Air mass 7 is quite moist in the subcloud layer, but convective potential is inhibited by the cool low-level temperatures (see Table 3).

The air mass differences described above have been subjectively evaluated by the authors to be significant and important with regard to mesoscale analysis and convective weather systems. Further comparison of the soundings plotted in Figs. 9 and 10 reveal some potentially serious problems in these VAS sounding applications. For example, the lapse rates in the 700–400 mb layer indicated by the VAS retrievals in Figs. 9b and 9c are much larger than the lapse rates for this layer as measured by the radiosondes (Figs. 10b and 10c). The lapse rate differences act to overestimate the available buoyant energy indicated by the VAS retrievals.

Previous studies have documented various consistent biases inherent in satellite retrievals which have not yet been fully resolved (Phillips et al., 1979; Schlatter, 1981; Smith et al., 1981; Jedlovec, 1984). The air mass analysis procedure described above minimizes the effect of any VAS sounding biases by reliance on differences among VAS retrievals. *Satellite soundings have shown considerably more skill in measuring gradients rather than absolute magnitudes of geopotential, temperature and dewpoint.* The analyst should therefore utilize VAS datasets to locate maxima (minima) and gradients of a parameter and rely on additional observations when a more precise measurement of temperature and dew-

TABLE 3. Mesoscale air mass characteristics from conventional data sources.

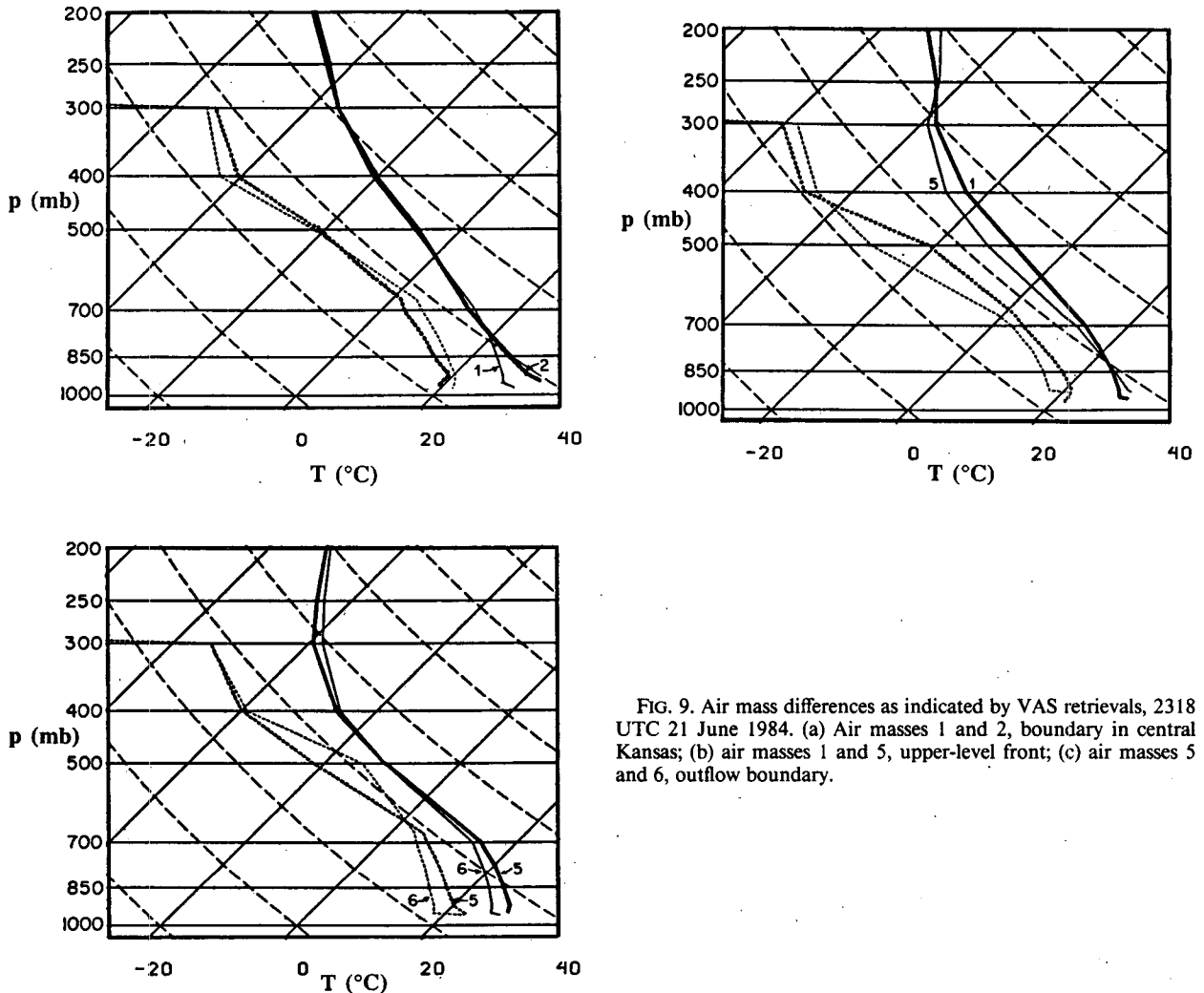| Air mass	Description	Surface temperature (°F)	Surface dewpoint (°F)	Average 500 mb temperature (°C)
1	capped, very moist	83–88	70–75	−8
2	hot, moist	93–97	62–67	−7
3	hot, dry	88–97	48–62	−8
4	very warm, very dry	82–92	35–48	−11
5	warm, moist, cold aloft	83–92	62–70	−12
6	rain cooled, subsidence	65–81	62–68	−12
7	cool, very moist	78–82	68–72	−8

FIG. 9. Air mass differences as indicated by VAS retrievals, 2318 UTC 21 June 1984. (a) Air masses 1 and 2, boundary in central Kansas; (b) air masses 1 and 5, upper-level front; (c) air masses 5 and 6, outflow boundary.

point is desirable. This approach is also advisable when analyzing VAS-derived thermodynamic parameters as shown in the next section.

Additional information about the mesoscale surface temperature distribution is available from the infrared imagery. A technique has been described by Weaver et al. (1985), in which detail is added to the temperature analysis from the 11.2 micrometer infrared window brightness temperatures at 8-km resolution.

c. VAS-derived thermodynamic parameters

An analysis of the type shown in section 3b may not be possible given the operational constraints of many forecasters. However, the VAS-derived thermodynamic parameters (section 2d) can quickly be computed and analyzed. Figures 11 and 12 show plots and analyses of VAS-derived positive area (CAPE or B) and negative area (N) respectively, derived from the same set of VAS retrievals used for the analysis in section 3b. The anal-

yses in Figs. 11 and 12 were done subjectively with considerable smoothing, and the VAS-derived parameters are somewhat noisy with a few obviously unrepresentative values. Nevertheless, a quantitative assessment of convective potential was produced which agrees with the qualitative description of the mesoscale air masses given in section 3b. Large values of positive area (CAPE or B) are associated with the very high dewpoints in the lowest kilometer of air mass 1, and also with the high cloud layer lapse rates (cool mid- and upper troposphere) in air mass 5. The regions which are dry in the lowest kilometer have low positive areas. The maximum negative area (N) values are found in air masses 1, 5 and 7 due to the more stable lapse rates in the lower layer.

As previously discussed, the positive areas assuming convective temperature (B_{CCL}) are computed to take into account boundary layer heating on the positive area (B). This is shown in Fig. 13 with analysis of both B and B_{CCL} at 1718 UTC. The B_{CCL} quantities are much
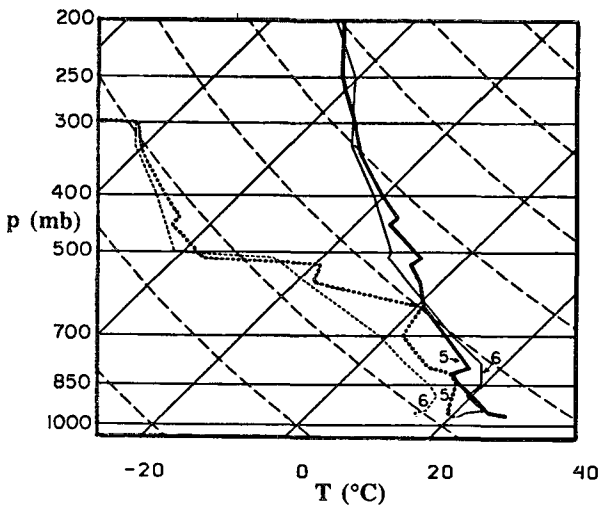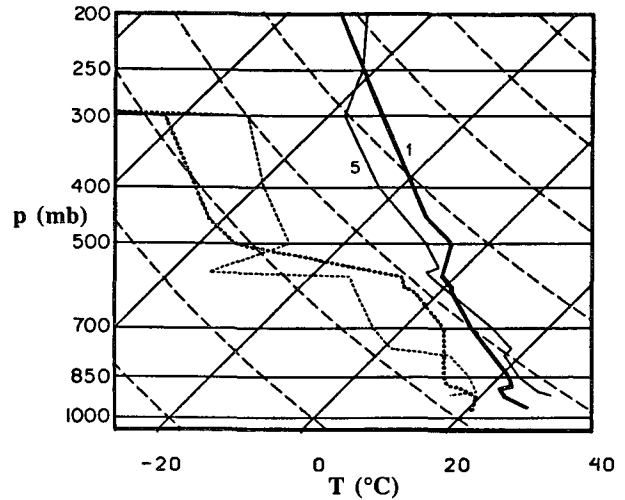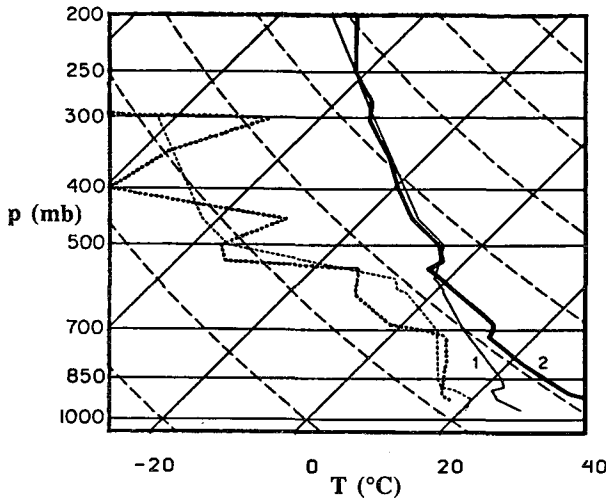
FIG. 10. Air mass differences corresponding to those in Fig. 9, as indicated by radiosonde observations. (a) Air mass 1, Monett, Missouri (UMN) and air mass 2, Dodge City, Kansas (DDC); 2315 UTC; boundary in central Kansas. (b) Air mass 1 (UMN) and air mass 5, North Platte, Nebraska (LBF); 2315 UTC; upper-level front. (c) Air mass 5, Omaha, Nebraska (OMA) at 2315 UTC and air mass 6, OMA at 0300 UTC; outflow boundary.
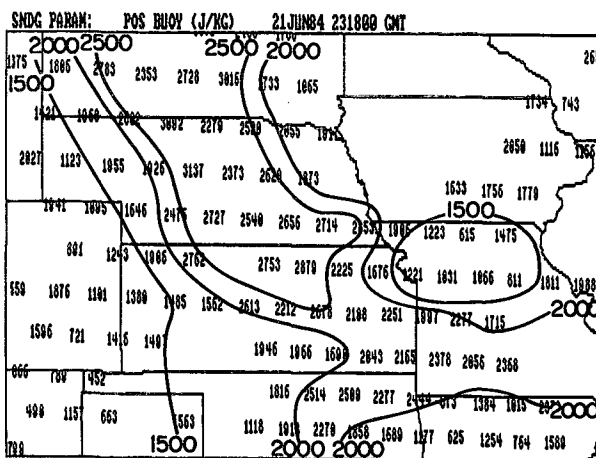

FIG. 11. VAS-derived positive buoyant energy, B (J kg^{-1}), also referred to as CAPE, 2318 UTC 21 June 1984.

higher than the B values and are comparable in magnitude to the 2318 UTC analysis of B shown in Fig. 11.

The four VAS-derived thermodynamic parameters defined in section 2d have been computed from the representative VAS retrievals for each air mass (Fig. 6) and are listed in Table 4. Several radiosonde-derived quantities are shown for comparison. The quantities in Table 4 reflect the air mass features qualitatively described earlier and also the apparent overestimates of positive area from VAS noted in section 3b.

Additional useful information is available from VAS retrievals due to their frequent time interval. The combined influences of advection, vertical motion, and diabatic heating (cooling) can be assessed with a time sequence of VAS datasets. Also, when a particular mesoscale feature and its characteristics are identified in independent datasets, the analysis of that feature be-
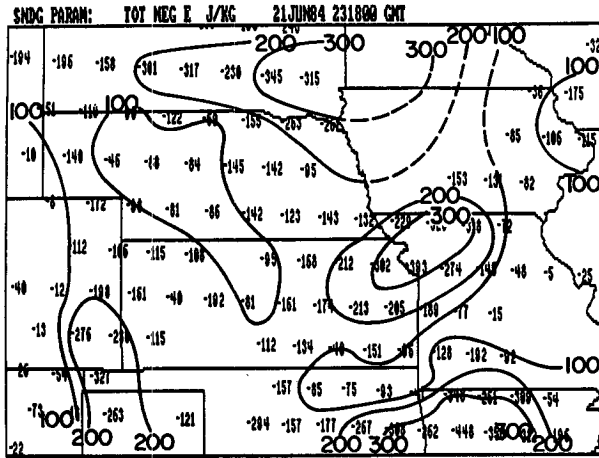
SNDG PARAM: TOT NEG E J/KG 21JUN84 231800 GMT

FIG. 12. VAS-derived negative buoyant energy, N (J kg^{-1}), 2318 UTC 21 June 1984.

TABLE 4. Characteristic derived thermodynamic parameters (J kg^{-1}) for each air mass type (Fig. 6) at 2315 UTC 21 June 1984.

Air mass	VAS average				Radiosonde			
	B	N	H	B_{CCL}	B	N	H	B_{CCL}
1	2316	242	285	3130	937	120	445	1774
2	1829	118	231	2560	—	—	—	—
3	1250	108	115	1513	993	59	283	1453
4	989	55	8	1002	—	—	—	—
5	2578	226	152	3053	1995	112	192	2600
6	1738	286	442	2730	462	345	400	1525
7	1145	215	415	2046	—	—	—	—

comes more credible. For example, the analysis procedure outlined in section 3b was applied to independent datasets at other time periods and produced similar analyses (not shown). The time continuity of the VAS data for this case study is illustrated in Fig. 14 showing the lowest kilometer dewpoint analysis for several time periods. Note the persistence of features such as the low-level moisture minimum in Missouri. The temporal continuity provided by VAS data is not available with the 12-hourly observations of the standard radiosonde network.

d. Diagnosis of the mesoscale convective systems

In order that a mesoscale analysis be truly useful, the information must be applicable to the diagnosis and prognosis of mesoscale convective systems (Mad-

dox, 1983; Rodgers et al., 1984). Forecast techniques of that type often require a careful reanalysis of routinely available data with emphasis on the mesoscale (Doswell, 1982). VAS retrievals offer a new data source with mesoscale space and time scales to supplement other data sources for optimum mesoscale air mass analysis. The analysis methods in this paper are proposed to aid in the diagnosis of thermodynamic and dynamic mechanisms pertinent to mesoscale convective systems.

During the afternoon of 21 June 1984, a severe thunderstorm formed in northwest Kansas along the boundary between air masses 1 and 3 (see Fig. 6 and the satellite image in Fig. 7). During the evening hours, this activity evolved into a mesoscale convective system in central and eastern Kansas. The infrared satellite image in Fig. 15 shows the eastern Kansas system near the time of its maximum extent. The Kansas MCS appeared to evolve and grow due to the high CAPE of air mass 1, yet required other mesoscale features for its initiation. A larger MCS developed in eastern Montana and propagated into western North Dakota, and
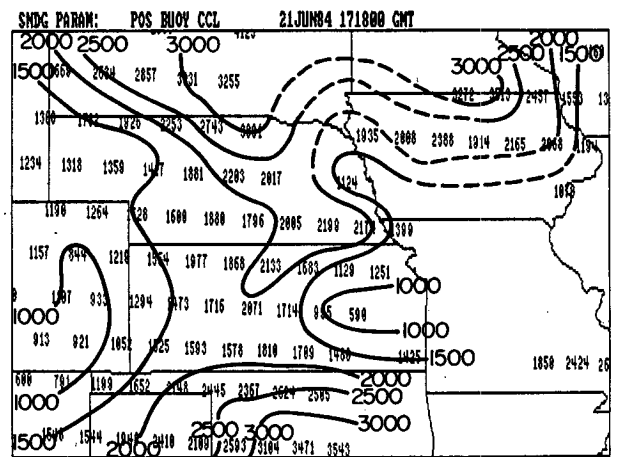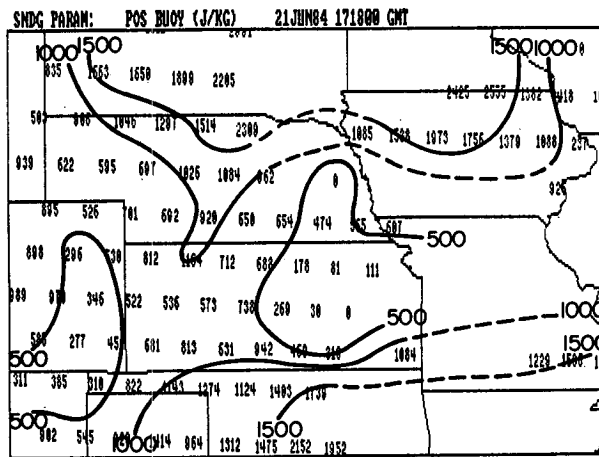
SNDG PARAM: POS BUOY (J/KG) 21JUN84 171800 GMT

SNDG PARAM: POS BUOY CCL 21JUN84 171800 GMT

FIG. 13. (a) VAS-derived positive buoyant energy, B (J Kg^{-1}), at 1718 UTC 21 June 1984. (b) VAS-derived positive buoyant energy at convective temperature, B_{CCL} (J Kg^{-1}), at 1718 UTC 21 June 1984.
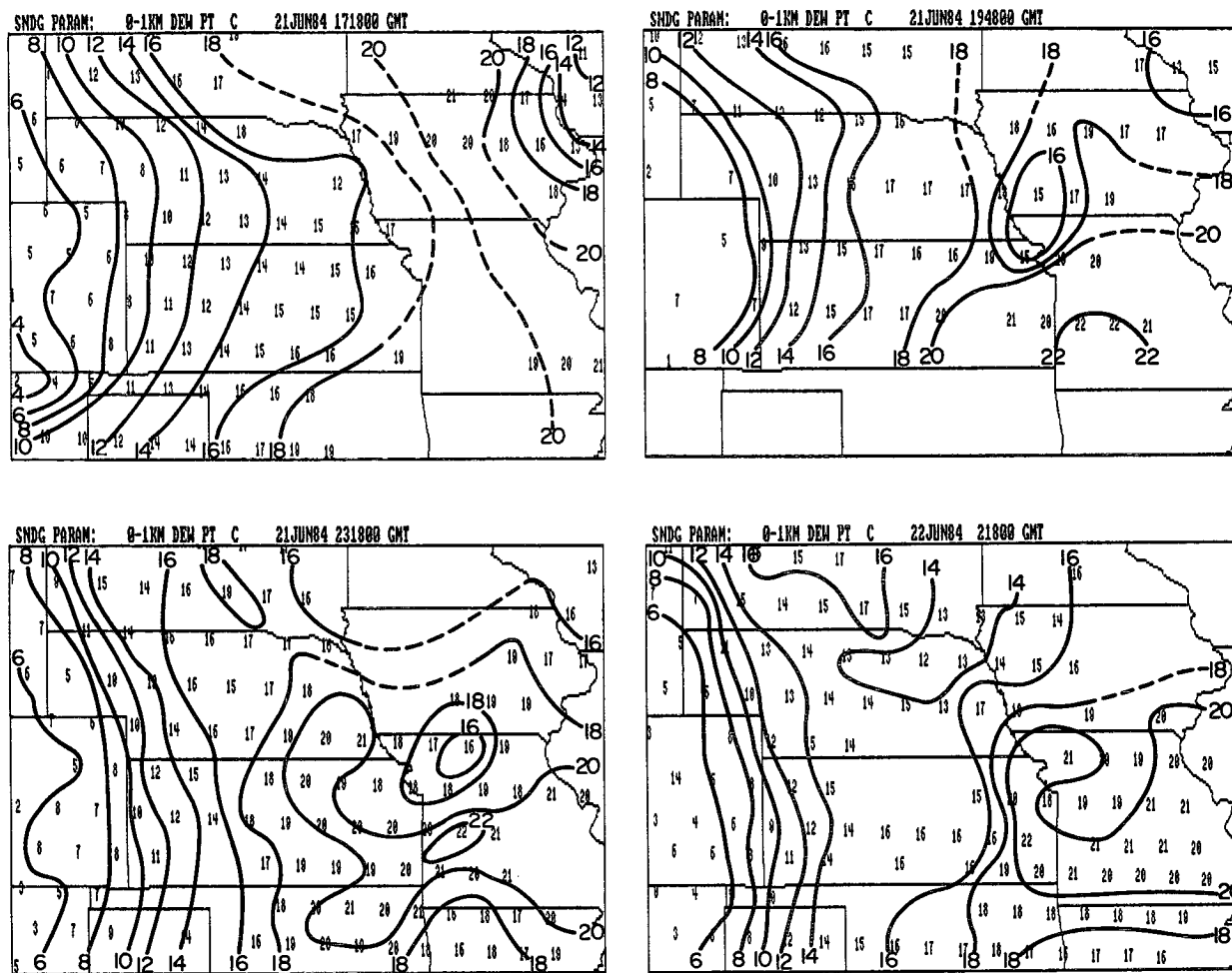
FIG. 14. VAS lowest kilometer dewpoint (°C) analyses. (a) 1718 UTC 21 June 1984; (b) 1948 UTC 21 June 1984; (c) 2318 UTC 21 June 1984; (d) 0218 UTC 22 June 1984.

another MCS formed in northeast Colorado. Each of these was supported by air mass 5.

This case study illustrates that VAS data, along with satellite imagery and conventional observations, can help delineate specific areas favorable for convective storm initiation. In addition, the fields of convective available potential energy (CAPE) can be portrayed with considerable detail.

4. Applications of VAS data to forecasting

a. Improvements in forecasting convective weather situations

In recent years, new observations, increased knowledge, and better technology have enhanced our ability to understand and predict mesoscale convective weather events (Ray, 1986). The contribution of VAS data to the detailed analysis shown in section 3 is an example of a means for improving forecasts. However, the information of air mass structure and distribution of available buoyant energy must be combined with additional data on large-scale dynamics, convergence fields, horizontal advection, etc. Therefore, requirements for utilizing VAS data to improve forecasts must include that the data be timely and easy to assimilate. The capability of transmitting VAS data and VAS-derived products to forecasters in the field for real-time applications has been clearly demonstrated (Wade et al., 1985; Birkenheuer and Snook, 1985; Purdom et al., 1985). One of the advantages of using VAS-derived thermodynamic parameters is that information pertinent to forecasting convective development and evolution can quickly be evaluated. The analyses of VAS thermodynamic parameters identify important mesoscale features, although individual quantities may be suspect due to VAS sounding biases and other data problems. Therefore, further improvement to meso-

FIG. 15. Infrared satellite image at 0530 UTC 22 June 1984.

scale convective forecasts attributed to VAS may be anticipated with increasing skill and experience in applying VAS-derived parameters, as well as improvements in the accuracy of retrievals.

b. Vertical distribution of water vapor

An accurate analysis of low-level water vapor is important input to forecasting thunderstorms and mesoscale convective systems. The convective available potential energy (CAPE) that fuels convective storm updrafts is strongly dependent on the amount of water vapor in the layer below cloud base. A simple sensitivity experiment with the CAPE quantities used in the previous section shows that the primary contributing factor to CAPE is the mixing ratio in the lowest kilometer. The spatial and temporal resolution of the conventional radiosonde network cannot adequately resolve the important mesoscale variance of moisture and temperature in the convective environment (Barnes and Lilly, 1975; Browning, 1980). Hillger and Vonder Haar (1981) have detected low-level mesoscale features with water vapor retrievals from the polar-orbiting High Resolution Infrared Sounder (HIRS) and such features are also detectable using VAS data.

Chesters et al. (1983) have proposed a method for deriving low-level water vapor fields from a pair of VAS channels. The algorithm is based on the different radiative properties of two VAS spectral bands (11.2 and 12.7 micrometers). This method (termed "split window") has been used to produce high resolution images of the water vapor patterns. Petersen et al. (1984) have combined images of this type with 6.7 micrometer VAS water vapor images to reveal patterns indicative of the vertical water vapor distribution.

Zehr (1986b) has shown an example to illustrate the utility of VAS retrievals in identifying very shallow moist layers. A few additional case studies (Petersen et al., 1984; Zehr, 1986a,b; Mostek et al., 1986; Robinson et al., 1986) have shown that VAS exhibits some skill in detecting the vertical distribution of water vapor. However, it remains to be demonstrated that VAS soundings can reliably and consistently measure the average mixing ratio in the layer below convective cloud base. This is particularly true considering the wide variety of temperature profiles which occur near the surface. Hayden et al. (1981) have pointed out the problems involved with deriving vertical water vapor profiles from satellite radiances. They illustrate the importance of using layer-averaged values when analyzing satellite soundings. Togstad et al. (1982) have proposed a method to improve the moisture structure of VAS retrievals.

Additional research aimed at improving the vertical profiles of VAS-derived water vapor amounts is needed. The VAS-derived thermodynamic parameters shown in this paper include the contribution of the low-level (0–1 km) water vapor only. The midlevel (above convective cloud base) water vapor amounts do not directly influence available buoyant energies (CAPE), but are very important in determining downdraft characteristics of convective storms (Knupp, 1987).

c. VAS comparisons with other types of information

Radiosonde observations and aircraft measurements offer the only "ground truth" data to assess the accuracy of VAS soundings. Sufficient aircraft data are not available. Ground-based radiometers may prove valuable in the future, but those soundings suffer from the same lack of vertical resolution as do satellite soundings (Hogg et al., 1983). An evaluation of VAS soundings based on comparisons with radiosonde data is therefore a necessary but difficult problem. It is important to be aware that although each data source is interpreted as a "vertical" profile of temperature and humidity, the sampling methods are vastly different. The radiosonde gives a point source measurement over a 30–45 minute ascent through the troposphere along a nonvertical path. VAS, on the other hand, samples a relatively large volume of air at a skewed viewing angle from geostationary altitude. For optimum mesoscale analyses, the two data sources should be complementary and not competitive. For example, VAS provides information on time changes and horizontal air mass extent not available from radiosondes. The location and magnitude of mesoscale horizontal temperature and moisture gradients can be specified by VAS. However, VAS cannot resolve fine vertical resolution structure such as the height of inversions and frontal surfaces. Since a radiosonde gives a point measurement, a question of representative area is naturally associated with each observation. The VAS information may help define uniform regions or air masses for which a radiosonde observation is valid.

Statistical correlations of vertical profiles from VAS and radiosondes, both for temperature and dewpoint, have been documented (Jedlovec, 1984; Fuelberg and Meyer, 1986). The differences between dewpoint measurements are quite large. The mesoscale analysis presented in this paper is strongly dependent on accurate dewpoint soundings. It has yet to be shown that VAS observations are sufficiently consistent and reliable in measuring convective potential and bulk thermodynamic parameters, and more studies of this type are needed. Improvements in retrieval algorithms should be assessed according to their effects on key thermodynamic parameters.

Surface observations and numerical model forecasts could be used to generate thermodynamic parameter fields independent of VAS measurements. Comparing those analyses with VAS-derived thermodynamic parameter analyses would give an evaluation of additional information from currently derived VAS datasets. A thorough study of this type on a daily basis has yet to be undertaken. However, the case study illustrated here and papers by Zehr (1986b) and Mostek et al. (1986) suggest that additional important thermodynamic information is indeed available from VAS.

5. Concluding remarks

The case study and analysis presented in this paper are shown to illustrate the potential of VAS soundings as a forecast tool and to propose new methods for their applications. With the anticipated operational use of VAS and the added capabilities of future GOES (GOES–NEXT), further development of forecast techniques utilizing VAS-derived thermodynamic parameters is needed. Additional refinements of information available from VAS, particularly in measuring temperature and moisture in the subconvective cloud layer, are necessary and should prove invaluable for mesoscale convective analyses. The next generation polar-orbiting satellites will carry advanced microwave sounding units which will have more channels and higher spatial resolution than the current microwave instruments (Heacock et al., 1986). The next generation geostationary satellite will have an improved sounding unit with the sounding and imaging function separated. The imager will be multichanneled, with higher resolution infrared data and improved rapid scan capability (Heacock et al., 1986).

The case study in this paper is intended to show how VAS data can currently be put to use. It is hoped that the discussion of these results will also shed some light on future applications of new satellite data to improve forecasts of convective storms.

REFERENCES

Barnes, S. L., and D. K. Lilly, 1975: Covariance analysis of severe storm environments. *Preprints Ninth Conf. on Severe Local Storms,* Norman, OK, Amer. Meteor. Soc., 301–306.

Birkenheuer, D., and J. S. Snook, 1985: A review of the VAS assessment during the 1985 PROFS summer exercise. NOAA Tech. Memo. ERL ESG-19, 80 pp.

Brandes, E. A., 1978: Mesocyclone evolution and tornadogenesis: Some observations. *Mon. Wea. Rev.,* **106,** 995–1011.

Browning, K. A., 1980: Review of local weather forecasting. *Proc. Roy. Soc. London,* A371, 197–211.

——, 1982: *Nowcasting.* Academic Press, 256 pp.

Byers, H. R., and R. R. Braham, Jr., 1949: *The Thunderstorm.* U.S. Govt. Printing Office, Washington, DC, 287 pp.

Chahine, M. T., 1968: Determination of the temperature profile in an atmosphere from its outgoing radiance. *J. Opt. Soc: Amer.,* **58,** 1634–1637.

Chesters, D., L. W. Uccellini and W. Robinson, 1983: Low-level water vapor fields from the VISSR Atmospheric Sounder (VAS) "split window" channels. *J. Climate Appl. Meteor.*, **22**, 725–743.

Cram, J. M., and M. L. Kaplan, 1985: Variational assimilation method and sensitivity experiments. *Mon. Wea. Rev.*, **113**, 467–484.

Doswell, C. A., III, 1982: The operational meteorology of convective weather. Volume I: Operational mesoanalysis. NOAA Tech. Memo. NWS NSSFC-5, 131 pp.

Fuelberg, H. E., and P. J. Meyer, 1986: An analysis of mesoscale VAS retrievals using statistical structure functions. *J. Climate Appl. Meteor.*, **25**, 59–76.

Fujita, T. T., 1963: Analytical mesometeorology: A review. *Meteor. Monogr.*, **5**(27), 77–125.

Green, R. N., and J. F. Weaver, 1985: Use of a personal computer workstation for short-range forecasting: A case study. *Proc. 14th Conf. on Severe Local Storms,* Indianapolis, Amer. Meteor. Soc., 97–100.

——, J. F. W. Purdom and D. A. Lubich, 1986: Assessment of a personal computer workstation for satellite meteorology. *Second Int. Conf. on Interactive Information and Processing Systems for Meteorology, Hydrology and Oceanography,* Miami, Amer. Meteor. Soc. 326–331.

Haltiner, G. J., and F. L. Martin, 1957: *Dynamical and Physical Meteorology.* McGraw-Hill, 470 pp.

Hayden, C., and P. Menzel, 1986: Description of VAS processing techniques. CIMSS Rep., SSEC, University of Wisconsin–Madison.

——, W. L. Smith and H. M. Woolf, 1981: Determination of moisture from NOAA polar-orbiting satellite sounding radiances. *J. Appl. Meteor.*, **20**, 450–466.

Heacock, E. L., Y. A. Afanasier, C. Horvault, T. Yoshida and U. V. G. Rao, 1986: Future world meteorological satellite systems. *Acta Astronaut.*, **14**, 277–285.

Hillger, D. W., and T. H. Vonder Haar, 1981: Retrieval and use of high-resolution moisture and stability fields from Nimbus-6 HIRS radiances in preconvective situations. *Mon. Wea. Rev.*, **109**, 1788–1806.

Hogg, D. C., M. T. Decker, F. O. Guiraud, K. B. Earnshaw, D. A. Merritt, K. P. Moran, W. B. Sweezy, R. G. Strauch, E. R. Westwater and C. G. Little, 1983: An automatic profiler of the temperature, wind, and humidity in the atmosphere. *J. Climate Appl. Meteor.*, **22**, 807–831.

Jedlovec, G. J., 1984: A statistical evaluation and comparison of VISSR Atmospheric Sounder (VAS) data and corresponding rawinsonde measurements. NASA Tech. Memo. 82575, NASA/MSFC, Huntsville, AL.

Knupp, K. R., 1987: Downdrafts within High Plains cumulonimbi. Part I: General kinematic structure. *J. Atmos. Sci.*, **44**, 987–1008.

Kreitzberg, C. W., 1976: Interactive applications of satellite observations and mesoscale numerical models. *Bull. Amer. Meteor. Soc.*, **57**, 679–685.

Lee, T. H., D. Chesters and A. Mostek, 1983: The impact of conventional surface data upon VAS regression retrievals in the lower troposphere. *J. Climate Appl. Meteor.*, **22**, 1853–1874.

Maddox, R. A., 1983: Large-scale meteorological conditions associated with midlatitude, mesoscale convective complexes. *Mon. Wea. Rev.*, **111**, 1475–1493.

Menzel, W. P., W. L. Smith and L. D. Herman, 1981: Visible infrared spin-scan radiometer atmospheric sounder radiometric calibration: An inflight evaluation from intercomparisons with HIRS and radiosonde measurements. *Appl. Opt.*, **20**, 3641–3644.

Miller, R. C., 1972: Notes on analysis and severe-storm forecasting procedures of the Air Force Global Weather Central. AWS Tech. Rep. 200. [NTIS AD-744 042.]

Mills, G. A., and C. M. Hayden, 1983: The use of high horizontal resolution satellite temperature and moisture profiles to initialize a mesoscale numerical weather prediction model--severe weather event case study. *J. Climate Appl. Meteor.*, **22**, 649–663.

Moncrieff, M. W., and J. S. A. Green, 1972: The propagation and transfer properties of steady convective overturning in shear. *Quart. J. Roy. Meteor. Soc.*, **98**, 336–352.

Mostek, A., L. W. Uccellini, R. A. Petersen and D. Chesters, 1986: Assessment of VAS soundings in the analysis of a preconvective environment. *Mon. Wea. Rev.*, **114**, 62–87.

NCAR, 1984: The National STORM Program, STORM-Central phase, preliminary program design. NCAR Rep., 147 pp.

Normand, C. W. B., 1938: On instability from water vapor. *Quart. J. Roy. Meteor. Soc.*, **64**, 47–69.

Petersen, R. A., L. W. Uccellini, A. Mostek and D. A. Keyser, 1984: Delineating mid- and low-level water vapor patterns in preconvective environments using VAS moisture channels. *Mon. Wea. Rev.*, **112**, 2178–2198.

Phillips, N., L. M. McMillin, A. Gruber and D. W. Wark, 1979: An evaluation of early operational temperature soundings from TIROS-N. *Bull. Amer. Meteor. Soc.*, **16**, 1188–1197.

Purdom, J. F. W., 1973: Mesohighs and satellite imagery. *Mon. Wea. Rev.*, **101**, 180–181.

——, 1982: Subjective interpretation of geostationary satellite data for nowcasting. *Nowcasting,* K. Browning, Ed., Academic Press, 149–166.

——, R. N. Green, J. F. Weaver, R. M. Zehr and D. A. Lubich, 1985: Satellite data support to the PRE-STORM Operations Center, May–June 1985. CIRA Pap. No. 3, Cooperative Institute for Research in the Atmosphere, Colorado State University, 75 pp.

Ray, P. S., Ed., 1986: *Mesoscale Meteorology and Forecasting.* Amer. Meteor. Soc., 793 pp.

Robinson, W. D., D. Chesters and L. W. Uccellini, 1986: Optimized retrievals of precipitable water fields from combinations of VAS satellite and conventional surface observations. *J. Geophys. Res.*, **91**, 5305–5312.

Rodgers, D. M., D. L. Bartels, R. D. Menard and J. H. Arns, 1984: Experiments in forecasting mesoscale convective weather systems. *Preprints Tenth Conf. on Weather Forecasting and Analysis,* Clearwater, Amer. Meteor. Soc., 486–491.

Schlatter, T. W., 1981: An assessment of operational TIROS-N temperature retrievals over the United States. *Mon. Wea. Rev.*, **109**, 110–119.

Smith, W. L., 1970: Iterative solution of the radiative transfer equation for temperature and absorbing gas profiles of an atmosphere. *Appl. Opt.*, **9**, 1993–1999.

——, 1983: The retrieval of atmospheric profiles from VAS geostationary radiance observations. *J. Atmos. Sci.*, **40**, 2025–2035.

——, and H. Woolf, 1984: Improved vertical soundings from an amalgamation of polar and geostationary radiance observations. *Preprints, Conf. on Satellite/Remote Sensing and Applications,* Clearwater, Amer. Meteor. Soc., 45–48.

——, —— and W. J. Jacob, 1970: A regression method for obtaining real-time temperature and geopotential height profiles from satellite spectrometer measurements and its application to Nimbus-3 "SIRS" observation. *Mon. Wea. Rev.*, **98**, 582–603.

——, V. E. Suomi, W. P. Menzel, H. M. Woolf, L. A. Sromovsty, H. E. Revercomb, C. M. Hayden, D. N. Erickson and F. R. Mosher, 1981: First sounding results from VAS-D. *Bull. Amer. Meteor. Soc.*, **62**, 232–236.

——, ——, F. X. Zhou and W. P. Menzel, 1982: Nowcasting applications of geostationary satellite atmospheric sounding data. *Nowcasting,* K. A. Browning, Ed., Academic Press, 123–135.

Suomi, V. E., T. Vonder Haar, R. Kraus and A. Stamm, 1971: Possibilities for sounding the atmosphere from a geosynchronous spacecraft. *Space Res.*, **11**, 609–617.

Togstad, W. E., J. M. Lewis and H. M. Woolf, 1982: A method for improving the estimation of conditional instability from satellite retrievals. NOAA Tech. Rep. NESS 93, 31 pp.

Velden, C. S., W. L. Smith and M. Mayfield, 1984: Application of VAS and TOVS to tropical cyclones. *Bull. Amer. Meteor. Soc.,* **65,** 1059–1067.

Wade, G. S., A. L. Siebers and R. W. Anthony, 1985: An examination of current atmospheric stability and moisture products retrieved from VAS measurements in real time for the NSSFC. *Preprints, 14th Conf. on Severe Local Storms,* Indianapolis, Amer. Meteor. Soc., 105–108.

Weather Research Program, 1984: Airborne Investigations of Mesoscale Convective Systems (AIMCS): Operational summary and data inventory. NOAA Tech. Memo. ERL ESG-9, 74 pp.

[Available from Environmental Science Group, NOAA/ERL, Boulder, CO 80303.]

Weaver, J. F., R. M. Zehr and J. F. W. Purdom, 1985: Mesoscale analysis of low-level temperature and water vapor distribution based on surface and satellite observations. *Preprints, 14th Conf. on Severe Local Storms,* Indianapolis, Amer. Meteor. Soc., 25–28.

Zehr, R. M., 1986a: Analysis of mesoscale air masses with VAS retrievals. *Preprints, Second Conf. on Satellite/Remote Sensing and Applications,* Williamsburg, Amer. Meteor. Soc., 347–350.

——, 1986b: Analysis of low-level water vapor fields. *Preprints, 11th Conf. on Weather Forecasting and Analysis,* Kansas City, Amer. Meteor. Soc., 330–334.